The EUMETSAT Satellite Application Facility on Land Surface Analysis (LSA SAF)

Algorithm Theoretical Basis Document (ATBD)

Down-welling Surface Shortwave Flux (DSSF)

PRODUCTS: LSA-201 (MDSSF) , LSA-202 (DIDSSF)

Reference Number: **SAF/LAND/MF/ATBD_DSSF/1.0**
Issue/Revision Index: **Issue 1.0**
Last Change: **20/11/2012**

DOCUMENT SIGNATURE TABLE

	Name		
Prepared by :	**Météo-France / CNRM**	**X/X/2012**	
Approved by :	**Land SAF Project Manager**	**X/X/2012**	

DOCUMENTATION CHANGE RECORD

Issue / Revision	Date	Description:
Version 1.0	**20/11/12**	**Preliminary version**

DISTRIBUTION LIST

Internal Consortium Distribution		
Organisation	**Name**	**No. Copies**
IM	Pedro Viterbo	
IM	Luís Pessanha	
IM	Isabel Trigo	
IM	Isabel Monteiro	
IM	Sandra Coelho	
IM	Carla Barroso	
IM	João Paulo Martins	
IM	Pedro Diegues	
IM	Benvinda Barbosa	
IM	Ana Veloso	
IDL	Carlos da Camara	
IDL	Teresa Calado	
IMK	Folke-S. Olesen	
IMK	Frank Goettsche	
MF	Jean-Louis Roujean	
MF	Xavier Ceamanos	
MF	Dominique Carrer	
RMI	Françoise Meulenberghs	
RMI	Arboleda Alirio	
RMI	Nicolas Ghilain	
UV	Joaquin Melia	
UV	F. Javier García Haro	
UV/EOLAB	Fernando Camacho	
UV	Aleixander Verger	

External Distribution		
Organisation	**Name**	**No. Copies**
EUMETSAT	Frédéric Gasiglia	
EUMETSAT	Dominique Faucher	
EUMETSAT	Lorenzo Sarlo	
EUMETSAT	Lothar Schueller	
EDISOFT	Teresa Cardoso	
EDISOFT	Carlos Vicente	
EDISOFT	Joaquim Araújo	
SKYSOFT	Mauro Lima	

Steering Group Distribution		
Nominated by:	**Name**	**No. Copies**
IM	**Carlos Direitinho Tavares**	**IM**
EUMETSAT	**Lorenzo Sarlo**	**EUMETSAT**
EUMETSAT	**Lothar Schueller**	**EUMETSAT**
EUMETSAT	**François Montagner**	**EUMETSAT**
STG/AFG (USAM)	**Francesco Zauli**	**STG/AFG (USAM)**
MF	**Jean-François Mahfouf**	**MF**
RMI	**Rafiq Hamdi**	**RMI**
KIT	**Herbert Fischer**	**KIT**

Table of Contents

List of Figures

List of Tables

1 Introduction

Down-welling surface short-wave radiation fluxes (DSSF) are generated on an operational basis by the EUMETSAT Satellite Application Facility (SAF) on Land Surface Analysis (LSA; Trigo et al., 2010). These products are derived from data acquired by the SEVIRI radiometer embarked on the Meteosat Second Generation (MSG) platform and delivered to the scientific community. There are two DSSF products, an instantaneous product every 30 minutes (LSA-201) and a daily product (LSA-202). Both products are computed from level 1.5 SEVIRI data corresponding the short-wave channels at 0.6 µm (VIS1), 0.8 µm (VIS2) and 1.6 µm (NIR). DSSF products are generated at full spatial resolution (3 km/pixel sampling distance at nadir), for 4 different geographical areas within the MSG disk (i.e., Europe, Northern Africa, Southern Africa and South America, see Figure 1).

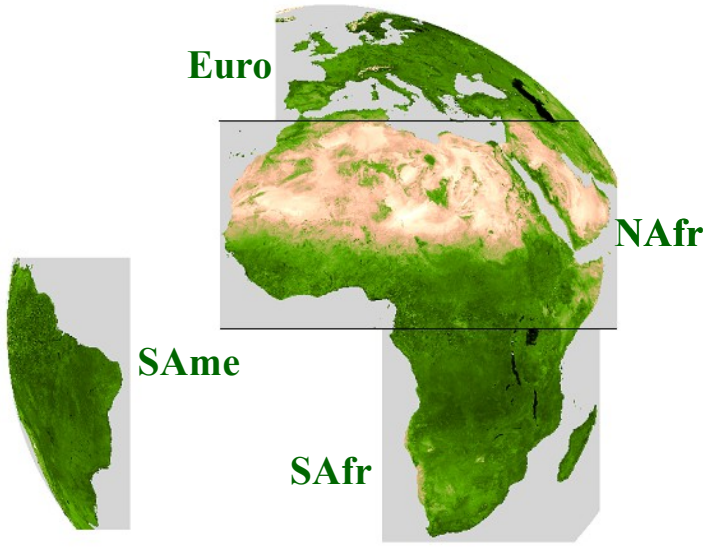

Figure 1 - The LSA SAF geographical areas for SEVIRI based products.

The down-welling surface short-wave radiation flux refers to the radiative energy in the wavelength interval [0.3 µm, 4.0 µm] reaching the Earth's surface per time and surface unit. It essentially depends on the solar zenith angle, on cloud coverage, and to a lesser extent on atmospheric absorption and surface albedo. An accurate knowledge of the distribution of solar radiation at the surface is essential for understanding climate processes at the Earth-atmosphere interface. The net radiation flux at the surface determines, to a large extent, such climate parameters as sensible and latent heat fluxes. It is also a key component in describing the spatial variability of biological processes and in validating climate models. Over the past few decades, the scientific community has developed computation methods for estimating both downward and net surface solar irradiance from satellite observations (e.g., Bishop et al., 1991; Darnell et al., 1988; Dedieu et al., 1987; Gautier et al., 1980; Gautier and Lansfeld, 1997; Li and Leighton, 1993; Masuda et

al., 1995; Moser and Raschke, 1984; Pinker and Ewing, 1985; Pinker and Laszlo, 1992; Tarpley, 1979; Whitlock et al., 1995).

The method for the retrieval of DSSF that is implemented in the LSA SAF system largely follows previous developments achieved at Météo-France in the framework of the OSI SAF (Brisson et al., 1999; Ocean & Sea-Ice, 2002). The main differences of the LSA SAF product are the spatial and temporal resolution, the source of ancillary input data, and the use of three short-wave SEVIRI channels (0.6 µm, 0.8 µm, and 1.6 µm).

The DSSF product of the LSA-SAF is produced from data acquired by the Spinning Enhanced Visible and Infrared Imager (SEVIRI) radiometer embarked on MSG. In the future, this product will be also produced for the Advanced Very High Resolution Radiometer (AVHRR) aboard the series of Metop satellites. Forecasts provided by the European Center for Medium-range Weather Forecasts (ECMWF) are used as ancillary data for the characterization of the atmosphere prior to estimation of the flux products.

The present document is one of the product manuals dedicated to LSA SAF users. The algorithm theoretical bases of the down-welling surface short-wave radiation flux generated by the LSA SAF are described in the following sections. The characteristics of the DSSF products derived from SEVIRI and provided by the LSA SAF are described in Table 2. Further details on the DSSF product requirements may be found in the Product Requirements Document (PRD) and the Product User Manual (PUM) which are available on the LSA SAF website.

Table 1 - Product Requirements for DSSF, in terms of area coverage, resolution and accuracy.

Product Name	Product Identifier	Coverage	Resolution		Accuracy		
			Temporal	Spatial	Threshold	Target	Optimal
MDSSF (DSSF SEVIRI)	LSA-201	MSG disk	30 min.	MSG pixel resolution	20%	DSSF>200 W/m2: 10% DSSF<200 W/m2: 20 W/m2	5%
DIDSSF (DSSF DAILY)	LSA-202	MSG disk	1 day	MSG pixel resolution	20%	DSSF>200 W/m2: 10% DSSF<200 W/m2: 20 W/m2	5%

2 Theoretical framework

The down-welling surface short-wave radiation flux $F^{\downarrow}$ is defined as the integral of the spectral irradiance $E(\lambda)$ over the wavelength interval [λ_1=0.3 µm, λ_2=4 µm]:

$$F^{\downarrow} = \int_{\lambda_1}^{\lambda_2} E(\lambda)\, d\lambda \quad . \tag{1}$$

The spectral irradiance is the hemispherical angular integral of the down-welling spectral radiance $L(\lambda, \theta, \varphi)$ weighted by the cosine of the zenith angle:

$$E(\lambda) = \int_0^{2\pi} \int_0^{\pi/2} L(\lambda, \theta, \varphi) \cos(\theta) \sin(\theta)\, d\theta\, d\varphi \quad . \tag{2}$$

It includes contributions owing to the direct solar radiation attenuated by the atmosphere as well as diffuse radiation.

In the applied retrieval scheme the DSSF is approximated as

$$F^{\downarrow} \approx F_0\, v(t) \cos\theta_s\, T \quad , \tag{3}$$

where F_0 is the solar constant (with minor corrections according to the restricted wavelength interval considered), θ_s the solar zenith angle, and T an effective transmittance of the atmosphere or cloud-atmosphere system. The factor

$$v(t) = 1 + 0.033 \cos(2\pi\, t/365) \tag{4}$$

takes into account the varying distance of the sun as a function of the day t of the year (Iqbal, 1983).

For the effective transmittance T different expressions are used depending on whether a given pixel is marked as clear or cloudy (see Figure 2). The information on cloud cover is provided by the cloud mask software that was developed by the NWC SAF and which is integrated in the LSA SAF operational system.

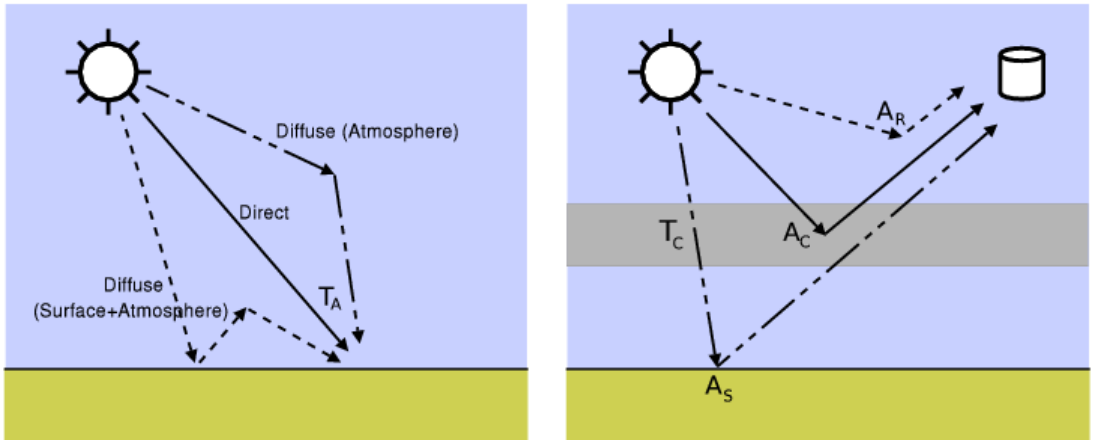

Figure 2: Schematics illustrating some elements of the clear (left) and cloudy sky (right) DSSF estimation methods.

3 Algorithm description

3.1 Overview

The proposed algorithm consists in calculating the effective transmittance T taking into account whether a given pixel is marked as clear or cloudy. Figure 3 shows a simplified flow chart of the algorithm. For clear and cloudy pixels quite different parametrizations are applied. The cloud mask therefore represents an important piece of information for the execution of the algorithm. In the presence of clouds the down-welling radiation reaching the ground is considerably reduced. The DSSF is strongly anti-correlated with the observable top-of-atmosphere reflectances, the brighter the clouds appear on the satellite images, the more radiation is reflected by them and the less radiation reaches the ground.

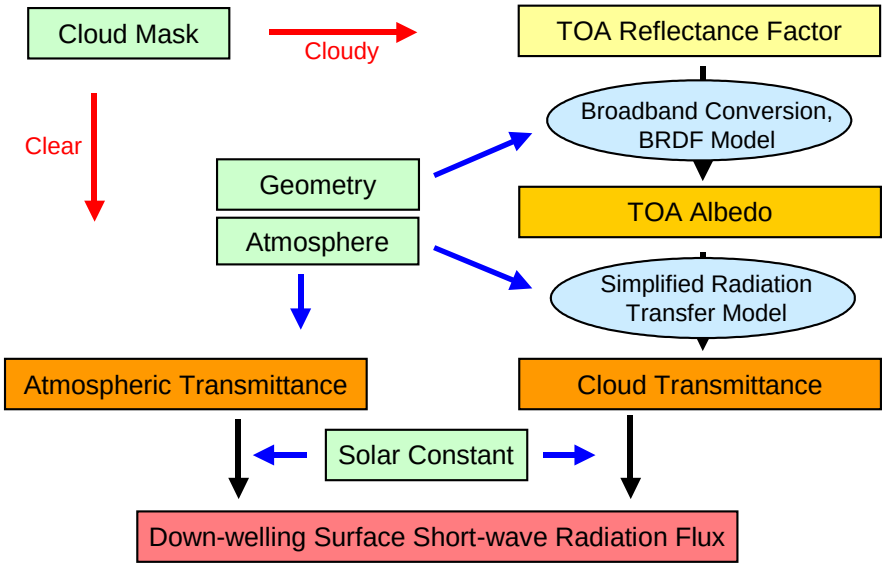

Figure 3: Simplified flow chart of the DSSF algorithm.

3.2 Clear sky method

In the case of clear pixels the factor T is specified as

$$T = T_A + \sum_{n=1}^{\infty} T_A \left(A_S A_A \right)^n = \frac{T_A}{1 - A_S A_A} \quad . \tag{5}$$

T_A represents the transmittance of the atmosphere and quantifies the contribution to the surface flux by the direct radiation as well as the diffuse radiation after scattering by the atmosphere as illustrated in the left diagram of Figure 2. The flux contribution owing to multiple scattering of the light between the surface and the atmosphere is taken into account by the denominator on the right-hand side of

Equation (5). A_S denotes the surface albedo and A_A the spherical albedo of the atmosphere. A_S indicated in the equation, the final form of this expression results from a geometric series taking into account an infinite number of scattering orders between surface and atmosphere.

The atmospheric transmittance is calculated after Frouin et al. (1989) as

$$T_A = e^{-\tau_{H2O}}\, e^{-\tau_{O3}}\, e^{-\tau_{Aer+CO2+O2}} \tag{6}$$

with

$$\tau_{H2O} = a_{H2O}\left(W/\cos\theta_s\right)^{b_{H2O}},\ \tau_{O3} = a_{O3}\left(U_{O3}/\cos\theta_s\right)^{b_{O3}}$$
$$\text{and } \tau_{Aer+CO2+O2} = \frac{1}{\cos\theta_s}\left(a + \frac{b}{V}\right)\ . \tag{7}$$

W is the water vapor column density in g/cm^2, U_{O3} the total ozone amount in atm.cm, and V the visibility in km. In the operational system the water vapor estimate is obtained from ECMWF numerical weather model forecasts and the ozone amount is specified according to the TOMS climatology. The visibility is currently kept at a fixed value of 20 km. The values of the parameters a and b were chosen according to the continental aerosol type.

The spherical albedo of the atmosphere $A_A = a' + b'/V$ is also parametrized as a function of visibility according to Frouin et al. (1989). The numerical values of the various constants are listed in the table below. The value used for F_0 is slightly lower than the solar constant since a restricted wavelength interval is considered in the definition of DSSF and in the radiative transfer calculations which served for setting up the optical thickness parametrizations (7). The surface albedo A_s is taken from the LSA SAF near real time albedo product (Land SAF, 2005). For the time being the bi-hemispherical variant A_{S-bh} is used and the diurnal cycle is approximated by using the functional form suggested by Dickinson (1983) and Briegleb et al. (1986) as

$$A_S = A_{S-bh}\frac{1+d}{1+2d\cos\theta_s} \quad \text{with } d = 0.4\ . \tag{8}$$

Table 2 - Numerical values of the constants appearing in the parametrizations of Frouin et al. (1989).

F_0	1358 W/m^2
a_{H2O}	0.102
b_{H2O}	0.29
a_{O3}	0.041
b_{O3}	0.57
a	0.066
b	0.704
a'	0.088
b'	0.456

3.3 Cloudy sky method

For cloudy pixels the DSSF estimate relies on a simplified physical description of the radiation transfer in the cloud-atmosphere-surface system according to Gautier et al. (1980) and Brisson et al. (1999). It is assumed that the whole image pixel is covered by a homogeneous cloud layer. The effective transmittance factor T is now given by

$$T = \frac{T_A T_C}{1 - A_S T_{bc} A_C} \quad . \tag{9}$$

Compared to the clear-sky case the enumerator additionally includes the cloud transmittance T_C, which is the decisive quantity in this expression. The denominator has a similar significance as in Equation (5) and quantifies multiple scattering between the surface and the bottom of the cloud layer. A_C denotes the cloud albedo and T_{bc} represents the atmospheric transmittance between the surface and the cloud.

The cloud transmittance T_C and albedo A_C may be highly variable on small time scales depending on the daily evolution of the clouds. Their instantaneous values are determined from the satellite measurements with the help of a simple physical model. For this purpose the measured spectral reflectances in the 0.6 µm, 0.8 µm, and 1.6 µm SEVIRI channels are first transformed to broad-band top-of-atmosphere albedo A_{TOA} by applying the spectral conversion relations proposed by Clerbaux et al. (2005) and the angular reflectance model of Manalo-Smith et al. (1998). As illustrated in the right diagram of Figure 3, the signal at the top of the atmosphere comprises contributions owing to Rayleigh scattering by the atmosphere above the cloud (A_R), radiation reflected by the cloud which is attenuated by the atmosphere above ($A_C T_{SunCloudSat}$), and radiation reflected by the surface which is attenuated by the atmosphere and the cloud ($A_S T_{SunSurfaceSat} T_C^2$):

$$A_{TOA} = A_R + A_C T_{SunCloudSat} + \frac{A_S T_{SunSurfaceSat} T_C^2}{1 - A_S T_{bc} A_C} \quad . \tag{10}$$

As before, the significance of the denominator in the third term is to take into account multiple scattering between the surface and the bottom of the cloud layer. Following Brisson et al. (1999) the transmittance factors $T_{SunCloudSat}$, $T_{SunSurfaceSat}$, and T_{bc}, as well as A_R are calculated with parametrizations given by Lacis and Hansen (1974). The cloud transmittance T_C is expressed in terms of the cloud albedo A_C and the cloud absorption a_C as

$$T_C = 1 - A_C - a_C = 1 - A_C - \alpha A_C \quad . \tag{11}$$

The cloud absorption is modeled as a linear function of the cloud albedo by introducing the “cloud absorption factor” α. The currently employed numerical value of $\alpha = 0.11$ was not derived from first principles, but has been adjusted by matching the final flux estimates with the help of a validation data base (Ocean & Sea-Ice, 2005). This parameter therefore mainly serves for “absorbing” the methodological

approximations and uncertainties, rather than for quantifying the physical cloud properties.

Combining the expressions (10) and (11) allows us to calculate the two unknowns T_C and A_C from the "observable" A_{TOA} by solving a quadratic equation, and finally to obtain the DSSF estimate with Equations (9) and (3).

The equation system gives a physical solution for T_C and A_C unless the "observed" value for A_{TOA} is beyond the following limits:

$$A_{TOA}^{\min} = A_R + A_S T_{SunSurfaceSat} \quad \text{corresponding to } T_C = 1 \tag{12}$$

$$A_{TOA}^{\max} = A_R + \frac{T_{SunCloudSat}}{1+\alpha} \quad \text{corresponding to } T_C = 0\,. \tag{13}$$

If the limiting conditions for the top-of-atmosphere albedo are violated, the cloud transmittance is set to the limiting value and a quality flag is set accordingly.

4 Known issues and limitations

- The DSSF product may contain spurious variability on short time scales, which may be caused by atmospheric effects like residual contamination by aerosols. Indeed, the load of aerosols is set to a constant visibility of 20 km. Bearing in mind possible lack of appropriate information on aerosol characteristics (load and type), future work will be carried out to produce DSSF products using different aerosol inputs (e.g., MACC-II forecast). In fact, MACC-II project appears to offer the necessary long-term perspectives to yield an improvement of the aerosol optical depth at 550 nm. Therefore, an even more positive impact on the accuracy assessment of the DSSF is reasonably foreseen is the near future. Besides, MACC-II re-analysis (from 2003) could be considered by the time of a LSA SAF products reprocessing.

5 References

Bishop, J. K. B., and Rossow, W. B., 1991. Spatial and temporal variability of global surface solar irradiance. Journal of Geophysical Research, 96, 16389 – 16858.

Briegleb B.P., P. Minnis, V. Ramanathan and E. Harrison, 1986, Comparison of Regional Clear-Sky Albedos Inferred from Satellite Observations and Model Computations, Journal of Applied Meteorology, 25, 2, 214-226.

Brisson A., Le Borgne P., Marsouin A., 1999, Development of Algorithms for Surface Solar Irradiance retrieval at O&SI SAF low and Mid Latitude, Météo-France/CMS, Lannion.

Clerbaux N., Bertrand C., Caprion D., Depaepe B., Dewitte S., Gonzalez L., Ipe A., 2005, Narrowband-to-Broadband Conversions for SEVIRI, Proceedings of the 2005 EUMETSAT Meteorological Satellite Conference, Dubrovnik, 351-357.

Darnell, W., Staylor, W., Gupta, S., and Denn, F., 1988. Estimation of surface insolation using sun-synchronous satellite data. Journal of Climate, 1, 820 – 835.

Dedieu, G. P., Deschamps, P., and Kerr, Y., 1987. Satellite estimation of solar irradiance at the surface of the earth and of surface albedo using a physical model applied to METEOSAT data. Journal of Climate and Applied Meteorology, 26, 79 – 87.

Dickinson R.E., 1983, Land surface processes and climate – Surface albedos and energy balance, Advances in Geophysics, 25, 305-353.

Ferranti, L. e P. Viterbo, 2006: The European Summer of 2003: Sensitivity of Soil Water Initial Conditions. J. Climate, 19, 3659-3680.

Frouin, R., D. W. Lingner, C. Gautier, K. S. Baker, and R. C. Smith, 1989, A simple analytical formula to compute clear sky total and photosynthetically available solar irradiance at the ocean surface, J. of Geophys. Res., 94, 9731-9742.

Gautier C., Diak G., Masse S., 1980, A simple physical model to estimate incident solar radiation at the surface from GOES satellite data, J. Climate Appl. Meteor., 19, 1005- 1012.

Gautier, C., and Landsfeld, M., 1997, Surface solar radiation flux and cloud radiative forcing for the atmospheric radiation measurement (ARM) southern great plains (SGP): a satellite, surface observations and radiative transfer model study. Journal of the Atmospheric Sciences, 54, 1289 – 1307.

Iqbal M., 1983, An Introduction to Solar Radiation, Academic Press, 390pp.

Lacis A.A., J.E. Hansen, 1974, A parametrization for the absorption of solar radiation in
the Earth's atmosphere, J. Atmos. Sci. 31, 118-133.

Land SAF, 2005, Land Surface Albedo Product User Manual, Version 1.3.

Land SAF, 2007, Product Output Format Document, SAF/LAND/IM/POF/2.0.

Li, Z., and Leighton, H. G. (1993). Global climatologies of the solar radiation budgets at the surface and in the atmosphere from 5 years of ERBE data. Journal of Geophysical Research, 98, 4919 – 4930.

Mitchell, K., et al., 2004: The multi-institution North American Land Data Assimilation System NLDAS: Utilizing multiple GCIP products and partners in a continental distributed hydrological modeling system, J. of Geophys. Res., doi:10.1029/2003JD003823.

Manalo-Smith N., G.L. Smith, S.N. Tiwari, W. F. Staylor, 1998, Analytic forms of bi-directional reflectance functions for application to Earth radiation budget studies, Journal of Geophysical Research, Vol. 103, D16, pp. 19, 733-19, 751.

Masuda, K., Leighton, H. G., and Li, Z. (1995). A new parameterization for the determination of solar flux absorbed at the surface from satellite measurements. Journal of Climate, 8, 1615 – 1629.

Moser, W., and Raschke, E. (1984). Incident solar radiation over Europe estimated from METEOSAT data. Journal of Climate and Applied Meteorology, 23, 166 – 170.

Nowcasting SAF, 2004, User Manual for the PGE01-02-03 of the SAFNWC/MSG: Scientific Part, Version 1.0. (latest version: 1.2, 2005)

Ocean & Sea Ice SAF, 2002, Surface Solar Irradiance Product Manual, Version 1.2.

Ocean & Sea Ice SAF, 2005, Surface Solar Irradiance Product Manual, Version 1.5.

Pinker, R., and Ewing, J. (1985). Modeling surface solar radiation: model formulation and validation. Journal of Climate and Applied Meteorology, 24, 389 – 401.

Pinker, R., and Laszlo, I. (1992). Modeling surface solar irradiance for satellite applications on a global scale. Journal of Applied Meteorology, 31, 194 – 211.

Schmetz, J., P. Pili, S. Tjemkes, D. Just, J. Kerkman, S. Rota, and A. Ratier (2002), An introduction to Meteosat Second Generation (MSG), Bull. Amer. Meteor. Soc., 83, 977-992.

Tarpley, J. (1979). Estimating incident solar radiation at the surface from geostationary satellite data. Journal of Climate and Applied Meteorology, 18, 1172 – 1181.

Trigo, I. F., C. C. DaCamara, P. Viterbo, J.-L. Roujean, F. Olesen, C. Barroso, F. Camacho-de-Coca, D. Carrer, S. C. Freitas, J. García-Haro, B. Geiger, F. Gellens-Meulenberghs, N. Ghilain, J. Meliá, L. Pessanha, N. Siljamo, A Arboleda (2010), The Satellite Application Facility on Land Surface Analysis, Int. J. Remote Sens., in press.

Whitlock, C. H., Charlock, T. P., Staylor, W. F., Pinker, R. T., Laszlo, I., Ohmura, A., Gilgen, H., Konzelman, T., DiPasquale, R. C., Moats , C. D., LeCroy, S. R., and Ritchey, N. A. (1995). First global WCRP shortwave surface radiation budget dataset. Bulletin of the American Meteorological Society, 76, 905 – 922.

Appendix A. Developers

The development and implementation of the DSSF algorithm have been carried out under the responsibility of the Centre National de Recherches Météorologiques (CNRM) of Météo-France (MF).

Authors: Bernhard Geiger, Catherine Meurey, Dulce Lajas, Laurent Franchistéguy, Dominique Carrer, Jean-Louis Roujean and Olivier Hautecoeur

Appendix B. Glossary

ATBD:	Algorithm Theoretical Basis Document
AVHRR:	Advanced Very High Resolution Radiometer
CNRM:	Centre National de Recherches Météorologiques
DSSF:	Down-welling Surface Short-wave Radiation
ECMWF:	European Centre for Medium-Range Weather Forecast
EPS:	EUMETSAT Polar System
EUMETSAT:	European Meteorological Satellite Organization
GOES:	Geo-stationary Operational Environmental Satellite
IM:	Instituto de Meteorologia (Portugal)
NIR:	Near Infrared Radiation
METEOSAT:	Geostationary Meteorological Satellite
METOP:	Meteorological Operational polar satellites of EUMETSAT
MF:	Météo-France
MSG:	Meteosat Second Generation
NWC:	NowCasting
NWP:	Numerical Weather Prediction
OSI:	Ocean and Sea Ice
SAF:	Satellite Application Facility
SEVIRI:	Spinning Enhanced Visible and Infrared Imager
TOMS:	Total Ozone Mapping Spectrometer